Simulation-Based Optimal Speed Control of PMSM Drives Using Discrete LQR with Integral Action: Design, Analysis, and Robustness Validation

Kittithuch Paponpen, **Tanapon Kumpao**, **Ekkachai Mujjalinvimut**, **Tirasak Sapaklom**, and **Mongkol Konghirun**†, Non-members

ABSTRACT

This paper presents a discrete-time linear quadratic regulator (LQR) augmented with integral action for high-performance speed control of permanent-magnet synchronous motor (PMSM) drives. Integral augmentation is embedded directly into the discrete-time LQR framework to eliminate steady-state error in both reference-speed tracking and load disturbance rejection. A discrete-time Lyapunov function is derived, with real-time evaluation under parametric uncertainty, to guarantee asymptotic stability of the closed-loop system. A MATLAB m-file implementation enables fine-grained tuning of sampling rates and seamless translation to embedded architectures. Robustness is assessed via a comprehensive simulation suite comprising step changes in speed reference, load-torque disturbances, ±10% variations in stator resistance and inductance, and ±15% variations in rotor inertia and viscous friction. Head-to-head benchmarking against a cascaded PI controller and a standard discrete-time LQR (without integral action) under identical scenarios quantifies improvements in convergence rate, overshoot, and disturbance-rejection performance. Simulation results demonstrate rapid convergence, minimal overshoot, and zero steady-state error, confirming the proposed method as a reliable, implementation-ready alternative for robust PMSM speed control.

Keywords: Discrete-Time LQR, Integral action, Lyapunov stability, Parametric uncertainty, PMSM speed control

1. INTRODUCTION

PMSMs are widely adopted in high-performance applications, including electric vehicles, robotics, and aerospace systems, owing to their superior torque density, efficiency, and dynamic performance [1] ,[2]. However, intrinsic nonlinearities and parameter sensitivity pose challenges for conventional control strategies, especially under varying load and parameter disturbances [3].

LQR control has emerged as a powerful solution for such systems, offering formal optimality through quadratic-cost minimization and ensuring closed-loop stability [4]. Discrete-time LQR design is particularly attractive in embedded and digital control, enabling efficient implementation on microcontrollers and digital signal processor (DSP) platforms. Nonetheless, classical LQR lacks integral action, which can yield nonzero steady-state errors when tracking references or rejecting disturbances [5]. To address this limitation, integral augmentation within the discrete-time LQR framework has been proposed, improving steady-state accuracy without sacrificing optimality [6], [7].

Recent advances in LQR applications have further improved PMSM speed control. In [8], a discrete-time LQR speed controller tailored for PMSMs is introduced, demonstrating stable and efficient regulation. Building on this, [9] proposes a continuous-time LQR speed control scheme that highlights the potential of optimal control in motor-drive systems. To address fixed-gain limitations, [10] and [11] explore intelligent tuning strategies such as the artificial-bee colony and other nature-inspired methods, for autotuning LQR gains under varying motor conditions. Disturbance handling has also been enhanced, for example, via feedforward compensation and state estimation [12], and by integrating disturbance observer or sliding-mode concepts into the LQR framework [13]. More recently, multithreaded LQR controllers have been reported for real-time state-feedback implementation in PMSM applications [14], reflecting interest in LQR-based strategies for embedded motor control platforms.

Despite these advances, systematic robustness analysis for discrete-time implementations remains underdeveloped, particularly with respect to parameter drift (e.g., stator resistance and inductance) and operational stresses (e.g., load-torque disturbances). Lyapunov-based stability analysis and real-time evaluation of a Lyapunov function have recently emerged as promising methods for validating theoretical guarantees and assessing controller performance under model uncertainties [15], [16].

This work adopts a fully discrete-time, simulation-driven methodology to close the gap between theoretical optimal control and practical embedded implementation.

Manuscript received on August 12, 2025; revised on September 20, 2025; accepted on October 2, 2025. This paper was recommended by Associate Editor Vuttipon Tarateeraseth.

The authors are with Department of Electrical Engineering, King Mongkut's University of Technology Thonburi, Thailand.

†Corresponding author: mongkol.kon@kmutt.ac.th

©2025 Author(s). This work is licensed under a Creative Commons Attribution-NonCommercial-NoDerivs 4.0 License. To view a copy of this license visit: https://creativecommons.org/licenses/by-nc-nd/4.0/.

Digital Object Identifier: 10.37936/ecti-eec.2525233.260765

Controller weights are selected via Bryson's rule to balance speed-tracking and control effort. A MATLAB m-file toolchain supports flexible sampling rate tuning, direct code generation for DSP/microcontroller targets, and real-time Lyapunov-function monitoring under parameter drift. Robustness is evaluated through scenario-based tests, reference steps, load-torque disturbances, ±10% stator-parameter and ±15% rotor-parameter variations. This end-to-end workflow provides a reproducible path from design to implementation and a fair basis for head-to-head comparisons with a cascaded PI, a non-integral discrete-time LQR, and the proposed LQR with integral action, evidencing gains in convergence rate, overshoot, and disturbance rejection. Accordingly, the main contributions of this paper are as follows.

1. Integral action is embedded in the discrete-time LQR framework for PMSM speed control, guaranteeing zero steady-state error in both reference-speed tracking and load-disturbance rejection.
2. A discrete-time Lyapunov function is derived, with real-time evaluation under parameter uncertainty to demonstrate asymptotic stability of the closed-loop system.
3. A MATLAB m-file implementation enables fine-grained tuning of sampling rates and direct translation to embedded architectures.
4. A comprehensive simulation suite, comprising step changes in the speed reference, load-torque disturbances, ±10% stator-parameter variations, and ±15% rotor-parameter variations, is used to assess robustness.
5. Comparative evaluation of a cascade PI controller, a discrete-time LQR without integral action, and the proposed integral-action LQR under identical scenarios is used to quantify improvements in speed-tracking accuracy and disturbance rejection.

The proposed approach bridges theoretical control design with practical implementation, targeting embedded applications where high-speed digital control of PMSM drives is required.

2. MODEL LINEARIZATION AND PLANT REPRESENTATION

2.1 Decoupling of Cross-Coupled Terms

In the dq frame, the PMSM voltage equations contain cross-coupling terms that complicate independent axis control. These terms are compensated using decoupling voltages [8]

$$u_{do} = -L_s p\omega_m i_q \tag{1}$$

$$u_{qo} = L_s p\omega_m i_d + p\omega_m \psi_f. \tag{2}$$

The actual control inputs are then

$$u_d = u_{dd} + u_{do} \tag{3}$$

$$u_q = u_{qq} + u_{qo}. \tag{4}$$

2.2 Continuous-Time Linearized Model

After applying decoupling and linearizing around the nominal point $(i_d^*, i_q^*, \omega_m^*) = (0, I_q^*, \omega_m^*)$, the PMSM is linearized to yield a decoupled continuous-time state-space model [10][11][17]

$$\frac{dx}{dt} = \mathbf{A}x(t) + \mathbf{B}u(t) + \mathbf{E}T_L(t) \tag{5}$$

with $x(t) = \begin{bmatrix} i_d(t) \\ i_q(t) \\ \omega_m(t) \end{bmatrix}$, $u(t) = \begin{bmatrix} u_{dd}(t) \\ u_{qq}(t) \end{bmatrix}$,

$$\mathbf{A} = \begin{bmatrix} -\frac{R_s}{L_s} & 0 & 0 \\ 0 & -\frac{R_s}{L_s} & 0 \\ 0 & \frac{3}{2}\frac{p\psi_f}{J_m} & -\frac{B_m}{J_m} \end{bmatrix}, \mathbf{B} = \begin{bmatrix} \frac{1}{L_s} & 0 \\ 0 & \frac{1}{L_s} \\ 0 & 0 \end{bmatrix},$$

$$\mathbf{E} = \begin{bmatrix} 0 \\ 0 \\ -\frac{1}{J_m} \end{bmatrix}.$$

2.3 Discrete-Time Model via Zero-Order Hold

For real-time implementation, the model is discretized using zero-order hold (ZOH) with sampling time T_s. The discrete-time state-space model becomes

$$x[k+1] = \mathbf{A}_d x[k] + \mathbf{B}_d u[k] + \mathbf{E}_d T_L[k] \tag{6}$$

In the discrete-time state-space model, the state vector at time step$k$, denoted$x[k]$, comprises the system states, typically the d- and q-axis currents (A) and rotor speed (rad/s). The subsequent state at the next time step is represented by with the same unit composition. The control input vector $u[k]$consists of the decoupled voltages $[u_{dd}[k], u_{qq}[k]]^T$ (V). The load torque disturbance at step is expressed as $T_L[k]$ ($N{\cdot}m$). The model is governed by matrices $\mathbf{A}_d$, $\mathbf{B}_d$, and $\mathbf{E}_d$.

The discrete matrices are computed as $\mathbf{A}_d = e^{\mathbf{A}T_s}$, $\mathbf{B}_d = \int_0^{T_s} e^{\mathbf{A}\tau} d\tau \cdot \mathbf{B}$ and $\mathbf{E}_d = \int_0^{T_s} e^{\mathbf{A}\tau} d\tau \cdot \mathbf{E}$.

This discrete model is used as the plant in the design of the LQR controller in Section 3.

2.4 Space-Vector PWM and Average-Value Inverter Model

To bridge the LQR controller's output and the PMSM plant, this study employs an average-value modelling approach for both the space vector pulse width modulation (SVPWM) and the voltage source inverter (VSI). These models provide a computationally efficient interface suitable for control-oriented simulation and real-time implementation.

$\cdot$ *SVPWM*

At each discrete sampling instant k, the control law generates $u_d[k]$ and $u_q[k]$, which are then transformed

into the $\alpha\beta$ frame voltages, $u_\alpha[k]$ and $u_\beta[k]$, using the inverse Park transformation

$$\begin{bmatrix} u_\alpha[k] \\ u_\beta[k] \end{bmatrix} = \begin{bmatrix} cos(\theta_e[k]) & -sin(\theta_e[k]) \\ sin(\theta_e[k]) & cos(\theta_e[k]) \end{bmatrix} \begin{bmatrix} u_d[k] \\ u_q[k] \end{bmatrix}. \tag{7}$$

Where $\theta_e[k]$ is the electrical rotor angle at discrete time step k. The voltages $u_\alpha[k]$ and $u_\beta[k]$ are then converted into three-phase modulation indices, $m_a[k]$, $m_b[k]$, $m_c[k]$, using the average min-max SVPWM method as

$$\begin{bmatrix} m_a[k] \\ m_b[k] \\ m_c[k] \end{bmatrix} = \begin{bmatrix} \frac{u_a[k]-u_{offset}[k]}{V_{dc}} + 0.5 \\ \frac{u_b[k]-u_{offset}[k]}{V_{dc}} + 0.5 \\ \frac{u_c[k]-u_{offset}[k]}{V_{dc}} + 0.5 \end{bmatrix}. \tag{8}$$

Where, V_{dc} is the DC link voltage of the VSI and $u_a[k], u_b[k], u_c[k]$ are the phase-equivalent voltages derived from the $\alpha\beta$ frame via inverse Clarke transformation, and $u_{offset}[k]$ is the average of the maximum and minimum phase voltages at each sampling step. This method ensures balanced PWM duty cycles with reduced computational overhead.

· *Average Value Model of Inverter*

The inverter's three-phase output voltages, $v_a[k]$, $v_b[k]$, $v_c[k]$, are computed using the modulation indices

$$\begin{bmatrix} v_a[k] \\ v_b[k] \\ v_c[k] \end{bmatrix} = \frac{V_{dc}}{3} \begin{bmatrix} 2 & -1 & -1 \\ -1 & 2 & -1 \\ -1 & -1 & 2 \end{bmatrix} \begin{bmatrix} m_a[k] \\ m_b[k] \\ m_c[k] \end{bmatrix}. \tag{9}$$

This formulation ensures the sum of phase voltages remains zero, maintaining balanced three-phase operation.

3. DISCRETE LQR CONTROLLER DESIGN WITH INTEGRAL ACTION

3.1 Decoupling of Cross-Coupled Terms

The discrete LQR controller is designed for the linearized, decoupled PMSM model in real units as shown in (6). The objective is to determine the state feedback control law as (10). that minimizes the infinite-horizon quadratic cost function in (11).

$$u[k] = -\mathbf{K}x[k] \tag{10}$$

$$\mathbf{J} = \sum_{k=0}^{\infty} (x[k]^T \mathbf{Q} x[k] + u[k]^T \mathbf{R} u[k]) \tag{11}$$

Where, $\mathbf{K}$ denotes the state feedback gain matrix designed using the LQR method. The symbol $\mathbf{J}$ represents the cost function that the LQR controller aims to minimize. The matrix $\mathbf{Q}$ is the state weighting matrix, which penalizes deviations of the system states, while $\mathbf{R}$ is the input weighting matrix, which penalizes excessive control effort. With $\mathbf{Q} \geq 0$ and $\mathbf{R} > 0$, The optimal gain matrix $\mathbf{K}$ is obtained by solve the discrete algebraic Riccati equation (DARE) [19],

$$\begin{aligned} \mathbf{P} = {} & \mathbf{A}_d^T \mathbf{P} \mathbf{A}_d \\ & - \mathbf{A}_d^T \mathbf{P} \mathbf{B}_d (\mathbf{R} + \mathbf{B}_d^T \mathbf{P} \mathbf{B}_d)^{-1} \mathbf{B}_d^T \mathbf{P} \mathbf{A}_d \ + \ \mathbf{Q}. \end{aligned} \tag{12}$$

The optimal feedback gain is

$$\mathbf{K} = (\mathbf{R} + \mathbf{B}_d^T \mathbf{P} \mathbf{B}_d)^{-1} \mathbf{B}_d^T \mathbf{P} \mathbf{A}_d. \tag{13}$$

While this LQR controller optimizes transient performance, it does not inherently eliminate steady state errors for step speed references. To achieve zero steady state error, an integral action is incorporated by augmenting the system with an integral state of the speed error

$$x_I[k+1] = x_I[k] + T_s(\omega_m^*[k] - \omega_m[k]). \tag{14}$$

The augmented state vector becomes

$$x_{aug}[k] = \begin{bmatrix} x[k] \\ x_I[k] \end{bmatrix} = \begin{bmatrix} i_d[k] \\ i_q[k] \\ \omega_m[k] \\ x_I[k] \end{bmatrix}. \tag{15}$$

Finally, the augmented discrete-time system is written as

$$\begin{aligned} x_{aug}[k+1] = {} & \mathbf{A}_{aug} x_{aug}[k] + \mathbf{B}_{aug} u[k] + \\ & \mathbf{E}_{agu} \omega_m^*[k] + \mathbf{D}_{aug} T_L[k]. \end{aligned} \tag{16}$$

Where $\omega_m^*[k]$ denotes the speed reference at sample k. The augmented matrices are $\mathbf{A}_{aug} = \begin{bmatrix} \mathbf{A}_d & 0 \\ -\mathbf{C}_\omega T_s & 1 \end{bmatrix}$, $\mathbf{B}_{aug} = \begin{bmatrix} \mathbf{B}_d \\ 0 \end{bmatrix}$, $\mathbf{E}_{aug} = \begin{bmatrix} 0 \\ T_s \end{bmatrix}$, $\mathbf{D}_{aug} = \begin{bmatrix} \mathbf{E}_d \\ 0 \end{bmatrix}$, with $\mathbf{C}_\omega = \begin{bmatrix} 0 & 0 & 1 \end{bmatrix}$.

According to the augmented LQR controller is designed by solving the DARE for the augmented system, yielding the control law

$$u[k] = -\mathbf{K}_{aug} x_{aug}[k] = -\begin{bmatrix} \mathbf{K}_x & \mathbf{K}_I \end{bmatrix} \begin{bmatrix} x[k] \\ x_I[k] \end{bmatrix}. \tag{17}$$

This ensures optimal transient response and zero steady-state error for step speed references, providing a robust and high-performance PMSM speed control solution.

Moreover, unlike classical control methods where bandwidth is explicitly designed , the bandwidth of the discrete LQR controller is an implicit outcome of the trade-off between state regulation ($\mathbf{Q}$ and $\mathbf{R}$). The solution of the DARE inherently balances these factors, determining the controllers closed-loop bandwidth without requiring explicit bandwidth specification. Therefore, in this study, bandwidth is not directly designed but rather emerges as a result of the systematic tuning process.

3.2 Weight Selection via Bryson's Rule

The weighting matrices $\mathbf{Q}$ and $\mathbf{R}$ are systematically tuned using Bryson's rule [18]. It is critical to emphasize that the tuning of $\mathbf{Q}$ and $\mathbf{R}$ is performed on the augmented discrete-time PMSM model with integral action,

Require
State variables:
$x = [\, i_d,\ i_q,\ \omega_m,\ x_I \,]$,
$u = [\, u_{dd},\ u_{qq} \,]$.
Maximum acceptable values:
$x_{\max} = [\, i_{d,\max},\ i_{q,\max},\ \omega_{m,\max},\ x_{I,\max} \,]$,
$u_{\max} = [\, u_{dd,\max},\ u_{qq,\max} \,]$.
Ensure:
$\mathbf{Q} \in \mathbb{R}^{4\times4}$,
$\mathbf{R} \in \mathbb{R}^{2\times2}$.
Initialize:
$\mathbf{Q} \leftarrow 0_{4\times4}$,
$\mathbf{R} \leftarrow 0_{2\times2}$.
for $i = 1$**to**4 **do**
$\mathrm{Q}(i,i) \leftarrow \dfrac{1}{\left(x_{\max}(i)\right)^2}$
end for
for $j = 1$**to**2 **do**
$\mathrm{R}(j,j) \leftarrow \dfrac{1}{\left(u_{\max}(j)\right)^2}$
end for
return $\mathbf{Q}, \mathbf{R}$

***Fig. 1**: Bryson's Rule Tuning of **Q** and **R**.*

not on the nominal linearized model alone.

Bryson's rule assigns diagonal LQR weights as the inverse square of the maximum acceptable magnitudes of the states and inputs [20]. Fig.1 illustrates the implementation used to select the diagonal weighting matrices $\mathbf{Q}$ and $\mathbf{R}$. The state components are $x_i \in \{i_d, i_q, \omega_m, x_I\}$ for $i = 1, \ldots, 4$, and the input components are $u_j \in \{u_d, u_q\}$ for $j = 1, 2$. For each component, a maximum acceptable magnitude $x_{(\max,(i))}$ or $u_{(\max,(j))}$ is specified. The matrices $\mathbf{Q}$ and $\mathbf{R}$ are initialized as zero matrices of size 4×4 and 2×2, respectively. For each state index i,

$$Q_{(i,i)} = \frac{1}{x^2_{(max(i))}}. \tag{18}$$

For each input index j,

$$R_{(j,j)} = \frac{1}{u^2_{(max(j))}}. \tag{19}$$

This assignment satisfies Bryson's rule. Any unit-sized deviation of a state or input, relative to its specified maximum, contributes equally to the LQR cost.

3.3 PI Tuning to Match LQR Bandwidth and Damping

· *Closed-Loop Dynamics Equivalence with the LQR Baseline*

This subsection concerns the outer speed loop. The inner current loops (i_d, i_q) are tuned once by bandwidth separation (approximately 5 to 10 times faster than the speed loop) and kept identical across PI, LQR with and without integral action for a fair comparison. With a fast-inner current loop, the speed plant from torque (or i_q^*) to speed is well approximated by a first-order continuous model

$$\mathbf{G}(s) = \frac{K_t}{J_m s + B_m} = \frac{K}{\tau s + 1}, \tag{20}$$

where $K = \frac{K_t}{B_m}$ and$\tau = \frac{J_m}{B_m}$. To extract the damping ratio and natural frequency from the LQR step response, the signal is first normalized to a unit step. The damping ratio(ζ)is determined from the peak overshoot(M_p) using the standard second-order relation. The peak-to-peak interval (T_p)between successive maxima yields the damped frequency($\omega_d = \frac{2\pi}{T_p}$), from which the natural frequency follows as $\omega_n = \frac{\omega_d}{\sqrt{1-\zeta^2}}$. For effectively non-oscillatory responses, ω_n may be estimated from the 2% settling time (T_{settle}).

$$\zeta = \sqrt{\frac{(lnM_p)^2}{\pi^2 + (lnM_p)^2}}, \omega_n \approx \frac{4}{\zeta T_{settle}} \tag{21}$$

For a continuous PI controller, $\mathbf{C}(s) = K_p^{spd} + \frac{K_i^{spd}}{s}$, matching the unity-feedback characteristic

$$\tau s^2 + (1 + KK_p^{spd})s + KK_i^{spd} = s^2 + 2\zeta\omega_n s + \omega_n^2 \tag{22}$$

gives closed-form seed gains

$$K_p^{spd0} = \frac{2\zeta\omega_n J_m - B_m}{K_t}, K_i^{spd0} = \frac{\omega_n^2 J_m}{K_t} \tag{23}$$

Then, implementation is discrete

$$\mathbf{C}(z) = K_p^{spd} + K_i^{spd}\frac{T_s}{1 - z^{-1}} \tag{24}$$

and control output,

$$u[k] = u[k-1] + K_p^{spd}(e[k] - e[k-1]) + K_i^{spd}T_s e[k] \tag{25}$$

with output saturation and integrator anti-windup, where $e[k] = \omega^*[k] - \omega[k]$.

· *Two-Stage Tuning Procedure*

Step 1 Analytic initial gains: The speed-loop PI gains $K_p^{spd0}$and $K_i^{spd0}$are computed from (23) by using the LQR baseline (measured $t_r^{LQR}$and OS^{LQR}) together with the plant parameters J_m, $B_m$andK_t. This choice matches the LQR intended bandwidth and damping on the ideal (nominal) plant.

Step 2 Practical refinement: Candidate gains are evaluated in a neighborhood of the analytic initial values $K_p^{spd0}$and K_i^{spd0}. Let $\alpha_p \in [0.5, 3], \alpha_i \in [0.05, 1.5]$and set $K_p^{spd} = \alpha_p K_p^{spd0}, K_i^{spd} = \alpha_i K_i^{spd0}$. Each candidate is assessed using the discrete speed-loop model, which accounts for the inner-loop bandwidth, actuator saturation, and anti-windup. For each candidate, a speed step is simulated and the rise time t_r, percent

overshoot OS, and control-effort $RMS(u)$ are recorded. The implemented gains are those that minimize subject to practical constraints: no sustained saturation (e.g., > 50 ms) and classical robustness margins (phase margin $\geq$ 45°, gain margin $\geq$ 6 dB). The quantities t_r^{LQR} and OS^{LQR} are measured from the LQR baseline. The weights ω_1, ω_2,and ω_3 are nonnegative (typical values $\omega_1 = \omega_2 = 1, \omega_3 = 0.5$). The control-effort RMS used in J_{tune} is defined by

$$J_{tune} = \omega_1(t_r - t_r^{LQR})^2 + \omega_2(OS - OS^{LQR})^2 + \omega_3 RMS(u)^2, \tag{26}$$

$$RMS(u) = \sqrt{\frac{1}{N}\sum_{k=k_0}^{k_0+N-1} u[k]^2}, \tag{27}$$

where k_0 is the step index and $N = T_{settle}/T_s$.

4. STABILITY ANALYSIS

4.1 Stability of the Augmented Discrete-Time System

According to (15) - (17), the resulting in closed-loop system dynamics is represented as

$$x_{aug}[k+1] = (\mathbf{A}_{aug} - \mathbf{B}_{aug}\mathbf{K}_{aug})x_{aug}[k] + \mathbf{E}_{agu}\omega_m^*[k] + \mathbf{D}_{aug}T_L[k]. \tag{28}$$

For stability analysis, focusing on the homogeneous system without external inputs is considered as

$$x_{aug}[k+1] = (\mathbf{A}_{aug} - \mathbf{B}_{aug}\mathbf{K}_{aug})x_{aug}[k]. \tag{29}$$

4.2 Lyapunov Stability Proof

The stability of the closed-loop system is analyzed by constructing a Lyapunov candidate function based on the solution $\mathbf{P} > 0$ of the DARE

$$\mathbf{P} = \mathbf{A}_{aug}^T\mathbf{P}\mathbf{A}_{aug} - \mathbf{A}_{aug}^T\mathbf{P}\mathbf{B}_{aug}(\mathbf{R} + \mathbf{B}_{aug}^T\mathbf{P}\mathbf{B}_{aug})^{-1}\mathbf{B}_{aug}^T\mathbf{P}\mathbf{A}_{aug} + \mathbf{Q}. \tag{30}$$

The Lyapunov function is defined as

$$\mathbf{V}(x_{aug}) = x_{aug}^T\mathbf{P}x_{aug}. \tag{31}$$

This function is positive definite for all $x_{aug} \neq 0$ with $\mathbf{P} > 0$. The discrete Lyapunov inequality is satisfied

$$\mathbf{V}(x_{aug}[k+1] - \mathbf{V}x_{aug}[k]) = x_{aug}[k]^T((\mathbf{A}_{aug} - \mathbf{B}_{aug}\mathbf{K}_{aug})^T\mathbf{P}(\mathbf{A}_{aug} - \mathbf{B}_{aug}\mathbf{K}_{aug}) - \mathbf{P}) x_{aug} < 0 \tag{32}$$

By using Lyapunov stability theorem, this ensures that

$$\lim_{k\to\infty} \mathbf{V}(x_{aug}[k]) \tag{33}$$

$$\lim_{k\to\infty} (x_{aug}[k]) \tag{34}$$

Therefore, the closed-loop augmented system under the designed LQR controller is asymptotically stable.

***Table 1**: Motor Parameters and Inverter Specifications.*

Symbol	Value	Unit
Motor parameters		
R_s	2.20	Ω
L_s	8.72	mH
J_m	3.17×10^{-5}	$kg\cdot m^2$
B_m	5.28×10^{-5}	$Nm\cdot s\cdot rad^{-1}$
p	4	-
ψ	0.0617	Wb
Rated Values		
I_{rated}	2.70	A_{rms}
$V_{llrated}$	200	V_{rms}
ω_{rated}	3000	rpm
T_{rated}	1.41	Nm
Inverter Specification		
V_{dc}	320	V
V_{max}	250	V
I_{max}	6	A

***Table 2**: LQR Controller Weights via Bryson's Rule.*

Variables	Value	Weight
$i_{d,max}$	6 A	$Q(1,1) = 2.78\times10^{-2}$
$i_{q,max}$	6 A	$Q(2,2) = 2.78\times10^{-2}$
ω_m	4500 rpm	$Q(3,3) = 4.938\times10^{-8}$
$x_{I,max}$	3000 rpm	$Q(4,4) = 1.11\times10^{-7}$
$u_{dd,max}$	250 V	$R(1,1) = 1.60\times10^{-5}$
$u_{qq,max}$	250 V	$R(2,2) = 1.60\times10^{-5}$

4.3 Stability under Parameter Uncertainty

In practical PMSM systems, parameters such as R_s, L_s, J_m and B_m are subjected to variations. These uncertainties can be modeled as additive perturbations, $\mathbf{A}_{aug} + \Delta\mathbf{A}$ and $\mathbf{B}_{aug} + \Delta\mathbf{B}$. The perturbed closed-loop system becomes

$$x_{aug}[k+1] = (\mathbf{A}_{aug} - \mathbf{B}_{aug}\mathbf{K}_{aug} + \Delta\mathbf{A} - \Delta\mathbf{B}\mathbf{K}_{aug})x_{aug}[k] \tag{35}$$

Stability is maintained if the perturbations are sufficiently small such that the Lyapunov inequality remains satisfied

$$(\mathbf{A}_{aug} - \mathbf{B}_{aug}\mathbf{K}_{aug} + \Delta\mathbf{A} - \Delta\mathbf{B}\mathbf{K}_{aug})^T\mathbf{P} (\mathbf{A}_{aug} - \mathbf{B}_{aug}\mathbf{K}_{aug} + \Delta\mathbf{A} - \Delta\mathbf{B}\mathbf{K}_{aug}) - \mathbf{P} < 0. \tag{36}$$

This condition defines the systems robust stability margin. For the designed LQR controller, theoretical guarantees and simulations confirm that stability is preserved for typical parameter uncertainties within $\pm$10%to $\pm$15%.

***Table 3**: Simulation Scenarios.*

Scenario	Description
S1	Step change in reference speed at noload condition from 0 to 1500 rpm at standstill and compare speed responses of PI, LQR without integral action, and LQR with integral action controllers.
S2	Step change in load from 0 to 1.41 Nm at 0.5 s during keeping constant reference speed at 1500 rpm and compare speed responses of PI, LQR without integral action, and LQR with integral action controllers.
S3	Combined step disturbance with step speed change from 0 to 1500 rpm and step torque change from 0 to 1.41 Nm at 0 s
S4	Parameter variation test with R_s and $L_s \pm 10\%$, J_m and $B_m \pm 15\%$

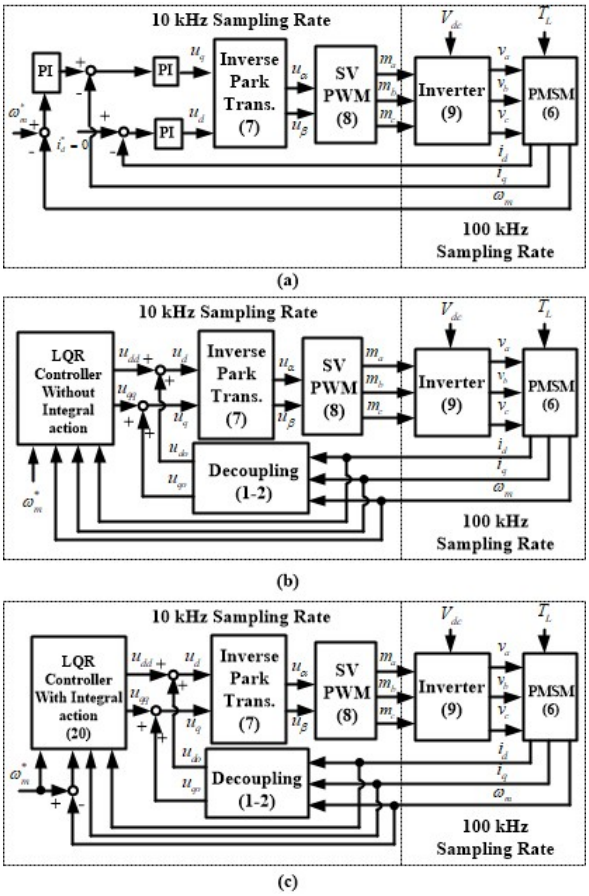

***Fig. 2**: Block Diagrams of the Three Discrete-Time PMSM Speed-Control Schemes: (a) Cascaded PI Controllers, (b) Standard LQR without Integral Action with Explicit Decoupling, (c) Proposed LQR with Integral Action.*

5. SIMULATION RESULTS AND PERFORMANCE VALIDATION

5.1 Simulation Framework

The PMSM model used in this study is based on a typical surface-mounted machine commonly employed in industrial applications. Table 1 summarizes the key rated parameters of the PMSM and the inverter specifications used for simulation studies. These parameters form the foundation for system modelling, controller design, and the selection of maximum acceptable values for the state and input variables in the Bryson's rule tuning process. The motors electrical and mechanical characteristics, along with the inverter's voltage and current limits, ensure that the simulation scenarios reflect realistic and practical operational conditions.

The maximum acceptable values for the state and input variables in Bryson's rule are selected based on the PMSMs rated parameters and practical operational limits. The current limits $i_{d,max}$ and $i_{q,max}$ are set slightly above the motors rated peak current to allow for transient conditions. The maximum rotor speed is set to $\omega_{m,max} = 1.5\omega_{rated}$ to provide an overspeed margin. The integral-state bound is chosen as $x_{I,max} = e_{max}T_{accum}$ with $e_{max} \approx \omega_{rated}$ and T_{accum} = 1 s. The maximum control signals $u_{dd,max}$ and $u_{qq,max}$ reflect expected controller output magnitudes and are distinct from the total motor voltages u_d and u_q which also include decoupling terms. This selection ensures a systematic and balanced LQR tuning aligned with realistic system constraints, as summarized in Table 2.

The simulation environment, implemented entirely in MATLAB m-files, adopts a multi-rate architecture as illustrated in Fig. 2. Three discrete-time speed control schemes - (a) cascaded PI controllers, (b) a standard LQR without integral action plus explicit decoupling, and (c) the proposed LQR with integral action - execute their control algorithms at a 10 kHz sampling rate, while the inverter and PMSM plant model run at 100 kHz to emulate typical SVPWM switching frequencies and capture high-frequency dynamics. This setup closely reproduces the timing and computational constraints of real-time digital control hardware, thereby ensuring that the design and performance validation remain practically relevant.

A series of simulation scenarios are designed to evaluate the controller's performance in speed tracking, disturbance rejection, and robustness under parameter variations. These scenarios, summarized Table 3, include step changes in reference speed, load torque, and combined disturbances.

Moreover, Table 4 summarizes the controller tuning parameters for the cascaded PI, discrete LQR, and discrete LQR with integral action schemes. For the PI controller, the table lists the proportional and integral gains for both the speed and current control loops. For the LQR-based controllers, the state weighting matrix **Q**, input weighting matrix **R**, and the integral state weighting q_I used in the LQR with integral action design are provided. The exact definitions of the **Q** and **R** matrices are given below the table, reflecting the trade-offs applied in the optimal control design to balance state regulation and control effort.

5.2 Speed Tracking Performance

Fig. 3 presents the speed tracking performance of the discrete LQR controller with integral action under a step

***Table 4**: Controller Tuning Parameters.*

Parameter	Cascaded PI	Discrete LQR	Discrete LQR + I
T_s [ms]	0.1	0.1	0.1
K_p^{spd0}	0.0430	–	–
K_i^{spd0}	11.10	–	–
K_p^{spd}	0.09	–	–
K_i^{spd}	1.5	–	–
K_p^i	3.0	–	–
K_i^i	15	–	–
Q	–	Q_{noI}	Q_I
R	–	R_{noI}	R_I
q_I	–	–	55.55

Q_{noI} = diag(2.50 × 10^5, 2.78, 39.50), R_{noI} = diag(16, 16)

Q_I = diag(111200, 0.2780, 0.0049), R_I = diag(0.064, 0.064)

Note: Closed-form initial gains were computed by matching the LQR baselines natural frequency and rise time (ω_n = 360 rad/s), $t_r \approx$ 5 ms); the implemented gains were then selected via the discrete-time refinement in (24) under saturation and robustness constraints.

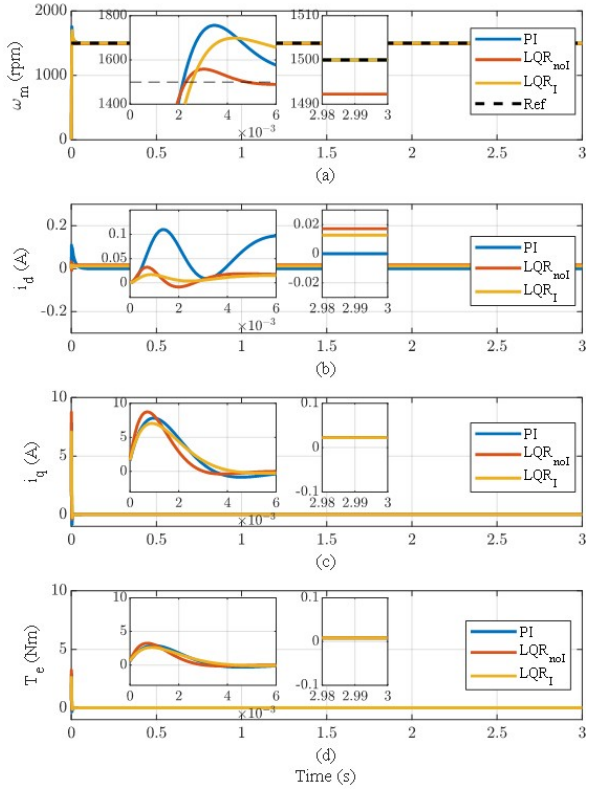

***Fig. 3**: Simulation Results for a No-Load Step-Speed Change to a 1500 rpm Reference: (a) Rotor Speed ; (b) D-axis Current ; (c) Q-axis Current ; and (d) Electromagnetic Torque . Responses are Shown for the PI Controller, Discrete-Time LQR without Integral Action (LQRnoI), and Discrete-Time LQR with Integral Action (LQRI).*

change in reference speed from 0 to 1500 rpm, starting rom standstill, in a no-load condition. Fig.3(a) shows the trade-off between transient response and steady-state accuracy. The cascaded PI controller delivers the fastest rise time of about 2 ms and zero steady-state error while producing the largest overshoot of roughly 17 percent. The standard discrete-time LQR slows slightly, reaching the setpoint in about 2.3 ms with overshoot near 3 percent, but retains a steady-state speed error of 10 rpm. The integral-action LQR arrives at the reference in around 2.5 ms with moderate overshoot of 12 percent and completely eliminates steady-state error, achieving an optimal balance between damping and accuracy.

In Fig. 3(b) the d-axis current transient peaks around 0.12 A for the cascaded PI, around 0.03 A for the LQR without integral action and around 0.016 A for the integral-augmented LQR. The PI loop exhibits modest oscillation before settling exactly to zero current. The standard LQR leaves a small steady bias of 0.015 A while the integral-augmented LQR returns to zero with the fastest damping.

In Fig. 3(c) the q-axis current overshoot reaches near 9.5 A for the PI controller, near 9 A for the LQR without integral action and near 8.5 A for the integral-augmented LQR before all three decay to zero in steady state. These results confirm that adding integral action both lowers peak currents and achieves exact current regulation under no-load conditions.

Fig. 3(d) depicts the electromagnetic torque T_e. A brief acceleration pulse occurs at the step (peak ≈ 4.5 N·m in the left inset), followed by a decay to a negligible steady level (right inset shows $|T_e| < 0.1$N·m). The cascaded PI trace exhibits the largest peak and a slight undershoot; the non-integral LQR peaks lower with a lightly damped tail; and the integral-action LQR gives the lowest peak and the fastest decay, yielding the smallest residual ripple. No sustained saturation is observed.

5.3 Disturbance Rejection Performance

Fig. 4 illustrates the systems response to a load torque disturbance of 1.41 Nm applied at t = 0.5 s while maintaining a constant reference speed of 1500 rpm. In Fig. 4(a), following the 0 to 1.41 Nm load torque step at 0.5 s, the PI controller exhibits a speed dip to 555 rpm, while the LQR with integral action controller reaches a similar minimum of 550 rpm. The LQR without integral action maintains a much smaller deviation, settling near 1050 rpm. In terms of recovery, the LQR with integral action controller demonstrates the fastest dynamic response, returning to within 5 rpm of the 1500 rpm reference in 35 ms. The PI controller follows with a slower recovery, reaching the same margin in 80 ms. The LQR without integral action fails to eliminate the steady-state error due to the absence of integral compensation.

The d-axis current responses in Fig.4(b) reveal distinct transient and steady-state behaviours. In the left inset, the PI controller shows a pronounced dynamic response with overshoot and undershoot, peaking near 0.15 A and dipping below zero before settling. Both LQR controllers exhibit fast responses with minimal transient deviation.

The LQR controllers, with and without integral action, reach their final values almost immediately and show no

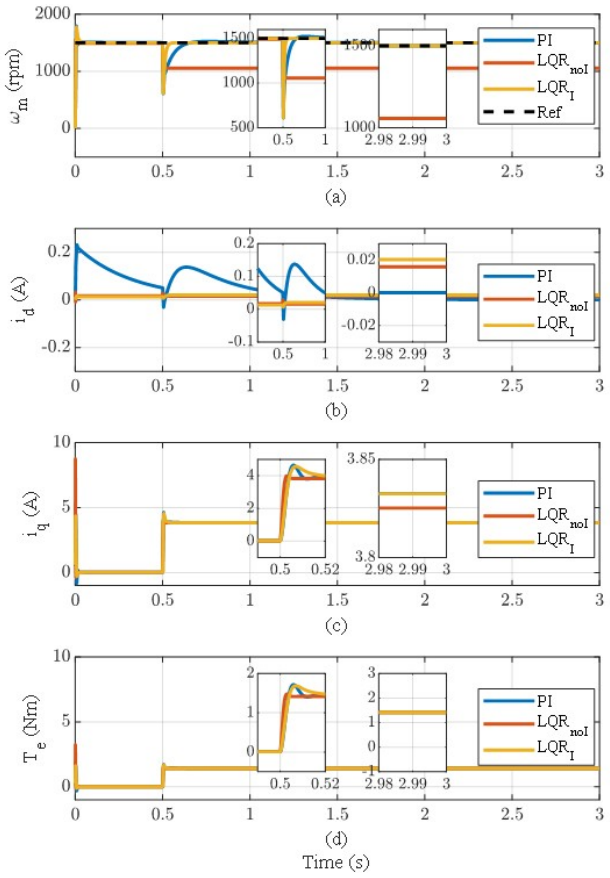

***Fig. 4**: Transient and Steady-State Responses to a Step Change in Load Torque from 0 to 1.41 Nm at 0.5 s with a 1500 rpm Speed Reference: (a) Rotor Speed ; (b) D-axis Current ; (c) Q-axis Current ; and (d) Electromagnetic Torque ; for PI, Discrete LQR without Integral Action and Discrete LQR with Integral Action Controllers.*

observable overshoot. In the steady state, as seen in the right inset, the PI controller converges to zero error while both LQR controllers maintain small but nonzero steady-state values, indicating a slight d-axis current offset under the same load condition. This nonzero d-axis current in both LQR controllers results from their control design, which does not explicitly regulate the d-axis current to zero but rather focuses on optimizing system states based on a predefined cost function.

In Fig. 4(c), the q-axis current responses reflect the torque demand required to maintain constant speed at 1500 rpm. In the left inset, the LQR without integral action exhibits the fastest rise time of 8 ms, while both the LQR with integral action controller and the PI controller follow with similar rise times of 10 ms. In terms of overshoot, the PI controller shows the highest at 5 A, followed by the LQR with integral action controller at 4.8 A, and the LQR without integral action with the lowest overshoot at 4 A. These differences result from the control characteristics. the LQR without integral action is designed for fast state feedback without accumulated error, leading to fast but lower amplitude response. The PI controller lacks optimal gain tuning, resulting in a higher overshoot. The LQR with integral action, although optimized and equipped with integral action, accumulates error more slowly at the beginning, slightly increasing overshoot. In the steady state, as shown in the right inset, all controllers settle to similar i_q values around 3.83 A, with slight deviations reflecting the balance between tracking performance and current regulation in each control design.

In Fig. 4(d), the electromagnetic torque T_e shows how the drive accommodates the applied load. At t = 0.5 s, the load step induces a brief transient above the final value (left inset); thereafter T_e converges to the imposed level of around 1.41 N·m with negligible ripple (right inset). The cascaded PI trace exhibits the largest peak with a small rebound; the nonintegral LQR produces the lowest peak but a slightly longer decay; and the integral-action LQR gives an intermediate peak with the shortest settling. No torque saturation is observed.

Fig. 5 presents the system response under a combined disturbance, where both the reference speed and the load torque experience step changes simultaneously. The speed reference is stepped from 0 to 1500 rpm, and the load torque T_L is stepped from 0 to 1.41 N·m at t = 0 s. Fig. 5(a) shows the motor speed ω_m tracking the reference speed ω_m^*. The controller achieves tr of approximately 0.1248 s, a t_s of 0.6466 s, and an overshoot of 2.83%. The ±2% bounds confirm that the speed stabilizes within acceptable limits after the transient, demonstrating the system's ability to handle simultaneous changes in speed reference and load torque.

Fig. 5(b) illustrates the i_q response, which quickly rises to approximately 3.8 A to supply the necessary torque for both speed tracking and load disturbance compensation. The i_q current stabilizes smoothly, indicating the controller's effective regulation of the torque-producing current. Fig.5(c) displays the load torque profile T_L, confirming the step change applied at t = 0 s.

These results validate the discrete LQR controller with integral action as a robust solution for simultaneous speed and load disturbances. The system exhibits fast transient performance, acceptable overshoot, and zero steady-state error, confirming the controller's suitability for practical PMSM drive applications.

5.4 Robustness Analysis

Fig. 6 presents the robustness evaluation of the discrete LQR controller with integral action under parameter uncertainties, defined as scenario S4 in Table 3. The analysis considers ±10%variations in the R_s and L_s, as well as ±15% variations in the J_m and B_m, relative to the nominal motor model. These perturbations are introduced independently, while maintaining a fixed operating point at 1500 rpm with no-load condition.

The main plot in Fig.6 illustrates the ω_m for each perturbed case in comparison to the nominal model. Across all cases, the system exhibits consistent and stable tracking of the reference speed. Although slight

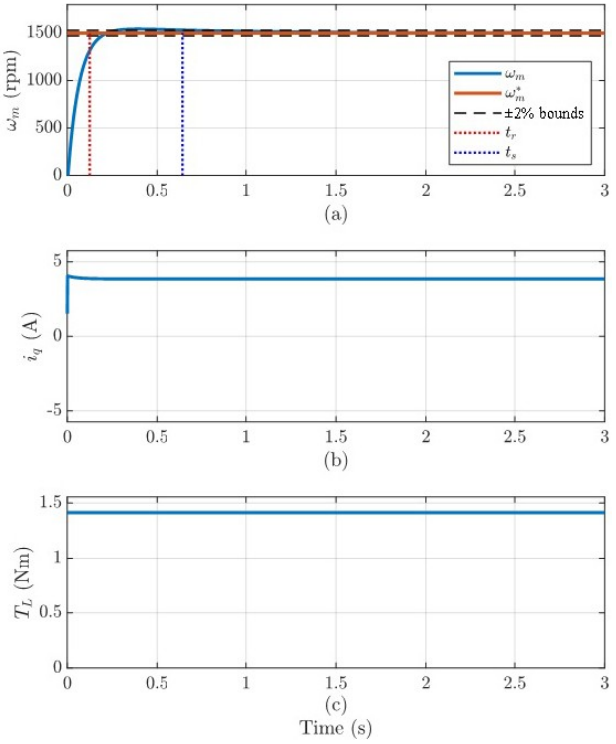

***Fig. 5**: System Response of the Discrete LQR Controller with Integral Action Under a Combined Step Disturbance: Reference Speed Step from 0 to 1500 rpm and Load Torque Step from 0 to 1.41 Nm at t = 0 s. (a) Motor speed an , with 2% bounds, and (b) response. (c) Load torque profile.*

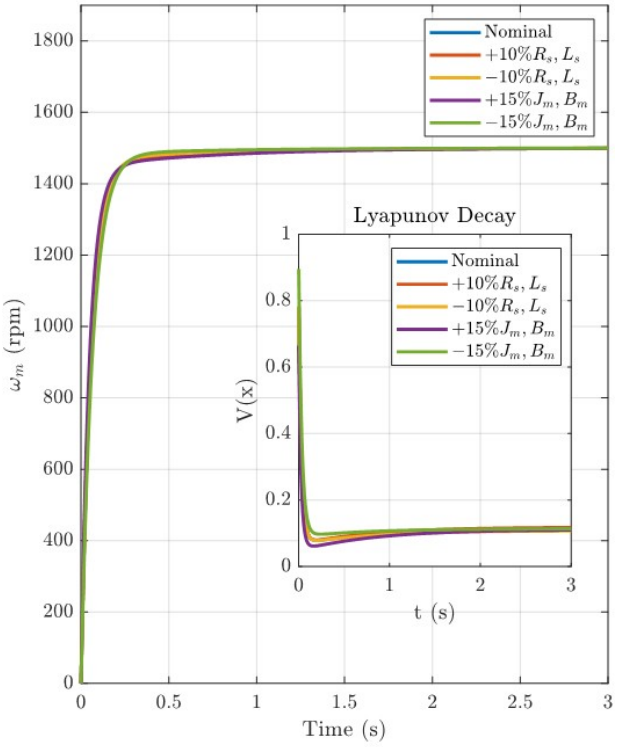

***Fig. 6**: Robustness Evaluation of the Discrete LQR Controller with Integral Action Under 10% Electrical and 15% Mechanical Parameter Variations*

differences in transient performance are observable, especially under variations in J_m and B_m, the overall settling behaviour remains within acceptable bounds, and all responses converge smoothly to the desired speed with negligible steady-state error. This confirms that the controller maintains performance robustness against realistic plant parameter deviations.

The inset plot shows the evolution of the Lyapunov function as shown in (31) , computed at each time step using the solution P of the DARE. The function demonstrates monotonic decay in all cases, validating the theoretical asymptotic stability of the closed-loop system despite the presence of parameter uncertainty.

Together, these results confirm that the proposed discrete LQR controller with integral action is robust not only in maintaining speed regulation but also in preserving closed-loop stability under bounded parametric deviations.

6. CONCLUSION

This paper presents the design and simulation-based evaluation of a discrete-time LQR controller with integral action for precise speed regulation of PMSM drives. The proposed method systematically addresses key challenges associated with digital control implementation and steady-state accuracy. First, the PMSM model is linearized and decoupled to enable state-space control formulation. The resulting continuous-time model is then discretized using a ZOH method to ensure compatibility with digital control platforms. An integral state is augmented to the system to eliminate steady-state speed tracking error. Finally, Bryson's rule is employed to systematically tune the LQR weighting matrices Q and R, ensuring balanced performance between state regulation and control effort.

Simulation results confirm that the proposed controller delivers precise speed tracking with fast settling and minimal overshoot, effectively rejects disturbances from sudden load torque variations, and maintains robust stability and performance under parameter deviations ranging from ±10% to ±15%. These findings confirm the effectiveness of the proposed controller in ensuring high-performance PMSM speed control within practical implementation constraints. The systematic tuning framework and simulation validation provide a solid foundation for future work, including experimental validation on hardware platforms and extension to sensorless control schemes.

NOMENCLATURE

i_d, i_q	dq-axis currents	$[A]$
u_d, u_q	control inputs in dq frame	$[V]$
u_{dd}, u_{qq}	decoupled control voltages in dq frame	$[V]$
u_{do}, u_{qo}	feedforward compensation voltages in dq frame	$[V]$
u	control effort	$[V]$
T_e	electromagnetic torque	$[N{\cdot}m]$
T_L	load torque	$[N{\cdot}m]$
R_s	stator resistance	$[\Omega]$
L_s	synchronous inductance	$[H]$
ψ_f	permanent-magnet flux linkage	$[Wb]$
p	pole pairs	$[-]$
e J_m	rotor inertia	$[kg \cdot m^2]$
B_m	viscous-friction coefficient	$[\frac{N{\cdot}m{\cdot}s}{rad}]$
K_t	torque constant	$[\frac{N{\cdot}m}{A}]$
θ_e	electrical rotor angle	$[rad]$
ω_m	mechanical speed	$[rad/s]$
u_α, u_β	control inputs in $\alpha\beta$ frame	$[V]$
m_a, m_b, m_c	modulation indices	$[-]$
V_{dc}	DC-link voltage	$[V]$
u_a, u_b, u_c	phase-equivalent voltages	$[V]$
v_a, v_b, v_c	phase voltages	$[V]$
u_{offset}	PWM offset voltage	$[V]$
V_{max}, I_{max}	inverter limits	$[V]$,$[A]$
I_{rated}	rated current	$[A_{rms}]$
ω_{rated}	rated speed	$[rpm]$
T_{rated}	rated torque	$[N{\cdot}m]$
ω_m^*	speed reference	$[rad/s]$
T_s	sampling period	$[s]$
$i_{d,max}, i_{q,max}$	current bounds for Bryson's rule	$[A]$
$\omega_{m,max}$	speed bounds for Bryson's rule	$[rpm]$
T_{accum}	error-accumulation horizon used to set $x_{I,max}$	$[s]$
$x_{I,max}$	integral-state bound for Bryson's rule	$[rpm]$
$u_{dd,max}, u_{qq,max}$	dq-voltage bounds for Bryson's rule	$[V]$
q_I	integral state weighting	$[-]$
ζ	damping ratio	$[-]$
τ	mechanical time constant	$[s]$
M_P	peak overshoot	$[-]$
T_P	peak-to-peak interval	$[s]$
ω_d	damped frequency	$[rad/s]$
ω_n	natural frequency	$[rad/s]$
T_{settle}	2% settling time	$[s]$
t_r	rise time	$[s]$
OS	percent overshoot	$[\%]$
K_P^{spd}, K_i^{spd}	speed-loop PI gains	$[-]$
K_P^{spd0}, K_i^{spd0}	analytic initial PI gains (LQR-matched)	$[-]$
e	tracking error $(\omega_m^* - \omega_m)$	$[rad/s]$
J_{tune}	tuning objective	$[-]$
t_r^{LQR}	t_r measured from the LQR baseline	$[s]$
OS^{LQR}	OS measured from the LQR baseline	$[\%]$
$\omega_1, \omega_2, \omega_3$	weights in J_{tune}	$[-]$
$RMS(u)$	control-effort used in J_{tune}	$[-]$
x	state vector	
x_{aug}	augmented state vector	
x_I	integral state	
$\mathbf{A}$	state transition matrix	
$\mathbf{B}$	input matrix	
$\mathbf{E}$	disturbance matrix	
$\mathbf{A}_d, \mathbf{B}_d, \mathbf{E}_d$	discrete-time matrices	
$\mathbf{K}$	state feedback gain matrix	
$\mathbf{J}$	LQR quadratic cost	
$\mathbf{R}$	input weighting matrix	
$\mathbf{Q}$	state weighting matrix	
$\mathbf{A}_{aug}, \mathbf{B}_{aug}, \mathbf{E}_{aug}$	augmented matrices	
$\mathbf{K}_{aug}$	augmented state feedback gain matrix	
$\mathbf{P}$	DARE solution	
$\Delta\mathbf{A}$,$\Delta\mathbf{B}$	additive model perturbations	
$\mathbf{V}(x_{aug})$	Lyapunov (value) function of the augmented state	
PMSM	permanent-magnet synchronous motor	
LQR	linear quadratic regulator	
PI	proportional-integral controller	
DSP	digital signal processor	
PWM	pulse width modulation	
SVPWM	space vector pulse width modulation	
VSI	voltage source inverter	
DARE	discrete algebraic Riccati equation	
ZOH	zero-order hold	

ACKNOWLEDGEMENT

This research project is supported by King Mongkut's University of Technology Thonburi (KMUTT), Thailand Science Research and Innovation (TSRI) , and National Science, Research and Innovation Fund (NSRF) Fiscal year 2027.

REFERENCES

[1] P. C. K. Luk, H. A. Abdulrahem, and B. Xia, "Low-cost high-performance ferrite permanent magnet machines in EV applications: A comprehensive review," *eTransportation*, vol. 6, Art. no. 100080, 2020.

[2] S. Boudouani, A. Yahdou, H. Benbouhenni, Z. Boudjema, M. M. Almalki, and T. A. Alghamdi, "Enhanced speed sensorless control of IPMSM

using integral synergetic observer," *Measurement and Control*, pp. 1–15, Jan. 2025.

[3] A. Loria, "Robust Linear Control of (Chaotic) Permanent-Magnet Synchronous Motors with Uncertainties," *IEEE Transactions on Circuits and Systems I: Regular Papers*, vol. 56, no. 9, pp. 2109-2122, Sept. 2009,

[4] A. Mukhatov, N. G. M. Thao, and T. D. Do, "Linear quadratic regulator and fuzzy control for grid-connected photovoltaic systems," *Energies*, vol. 15, no. 4, p. 1286, Feb. 2022.

[5] B. Kedjar and K. Al-Haddad, "DSP-Based Implementation of an LQR With Integral Action for a Three-Phase Three-Wire Shunt Active Power Filter," *IEEE Transactions on Industrial Electronics*, vol. 56, no. 8, pp. 2821-2828, Aug. 2009,

[6] D. Dewar, A. Formentini, K. Li, P. Zanchetta, and P. Wheeler, "Optimal and automated decentralised converter control design in more electrical aircraft power electronics embedded grids," *IET Power Electronics*, vol. 14, pp. 690–705, Jan. 2021.

[7] T. Jeon and I. Paek, "Design and verification of the LQR controller based on fuzzy logic for large wind turbine," *Energies*, vol. 14, no. 1, p. 230, Jan. 2021.

[8] L. M. Grzesiak and T. Tarczewski, "Permanent magnet synchronous motor discrete linear quadratic speed controller," in *2011 IEEE International Symposium on Industrial Electronics*, Gdansk, Poland, 2011, pp. 667-672.

[9] W.-J. Xu, "Permanent magnet synchronous motor with linear quadratic speed controller," *Energy Procedia*, vol. 14, pp. 364–369, 2012.

[10] T. Tarczewski and L. M. Grzesiak, "Artificial bee colony based auto-tuning of PMSM state feedback speed controller," in *2016 IEEE International Power Electronics and Motion Control Conference (PEMC)*, Varna, Bulgaria, 2016, pp. 1155 -1160.

[11] T. Tarczewski and L. M. Grzesiak, "An Application of Novel Nature-Inspired Optimization Algorithms to Auto-Tuning State Feedback Speed Controller for PMSM," *IEEE Transactions on Industry Applications*, vol. 54, no. 3, pp. 2913-2925, May - Jun. 2018.

[12] C. Xia, N. Liu, Z. Zhou, Y. Yan and T. Shi, "Steady-State Performance Improvement for LQR-Based PMSM Drives," *IEEE Transactions on Power Electronics*, vol. 33, no. 12, pp. 10622-10632, Dec. 2018.

[13] Z. Zhang, G. Yang, J. Fan, T. Li, and Q. Cai, "A disturbance sliding mode observer designed for enhancing the LQR current-control scheme of a permanent magnet synchronous motor," *Actuators*, vol. 13, no. 8, p. 283, Jul. 2024.

[14] [14] H. S and A. R. S, "State Feedback Speed Control of PMSM using Multithreaded Controller," in *2024 IEEE International Conference on Power Electronics, Drives and Energy Systems (PEDES)*, Mangalore, India, 2024, pp. 1-6.

[15] M. K. Bourdoulis, A. T. Alexandridis and J. J. Makrygiorgou, "Nonlinear Stability Analysis of Fully Controlled Permanent Magnet Synchronous Machines," in *2018 IEEE Conference on Control Technology and Applications (CCTA)*, Copenhagen, Denmark, 2018, pp.1191-1196.

[16] J. Zhang, W. Ren and X. -M. Sun, "Current-Constrained Adaptive Robust Control for Uncertain PMSM Drive Systems: Theory and Experimentation," *IEEE Transactions on Transportation Electrification*, vol. 9, no. 3, pp. 4158-4169, Sept. 2023.

[17] T. Tarczewski and L. M. Grzesiak, "Constrained State Feedback Speed Control of PMSM Based on Model Predictive Approach," *IEEE Transactions on Industrial Electronics*, vol. 63, no. 6, pp. 3867-3875, Jun. 2016.

[18] M. Latroch, A. Aissa-Bokhtache and A. Toualbia, "A Proposed Empirical Method of Weighing Matrices Determination in LQ Controller Applied," in *2023 2nd International Conference on Electronics, Energy and Measurement (IC2EM)*, Medea, Algeria, 2023, pp. 1 – 7.

[19] K. Suleimenov and T. D. Do, "Data-Driven LQR for Permanent Magnet Synchronous Machines," in *2019 IEEE Vehicle Power and Propulsion Conference (VPPC)*, Hanoi, Vietnam, 2019, pp. 1-5.

[20] N. Bouarroudj, Y. Houam, A. Djari, V. FeliuBatlle, A. Lakhdari, and B. Benlahbib, "A Linear Quadratic Integral Controller for PV-Module Voltage Regulation for the Purpose of Enhancing the Classical Incremental Conductance Algorithm," *Energies*, vol.16, no.11, pp.4532, 2023.

Kittithuch Paponpen received the M.Eng. degree in Electrical Engineering in 2007 and is currently pursuing a Ph.D. in Electrical and Computer Engineering at King Mongkut's University of Technology Thonburi (KMUTT), Thailand. Since 2007, he has been serving as a lecturer in the Department of Electrical Engineering at Silpakorn University (SU). His research interests include adjustable-speed drives, servo drive systems, and power electronics.

Tanapon Kumpao received the B.Eng. degree (First Class Honours) in Electrical Engineering from King Mongkut's University of Technology Thonburi, Bangkok, Thailand, in 2017. He earned the M.Sc. in Railway Systems Engineering and Integration and the Ph.D. in Electronic, Electrical and Systems Engineering from the University of Birmingham, Birmingham, United Kingdom, in 2019 and 2024, respectively. He is currently a Lecturer in the Department of Electrical Engineering, King Mongkut's University of Technology Thonburi. His research interests include electric motor drives for traction systems, electrotechnology for railway applications, condition monitoring, fault detection and diagnosis algorithm development, and renewable energy grid integration.

Ekkachai Mujjalinvimut received the B.Eng. and M.Eng. degrees in electrical engineering from King Mongkut's University of Technology Thonburi (KMUTT), Thailand, in 2007 and 2009, respectively, and the D.Eng. degree in electrical and information engineering technology from KMUTT in 2016. He is currently an Assistant Professor with the Department of Electrical Engineering, KMUTT. His research interests include power electronics and digital control of switched-mode power supplies and motor drives, with additional interest in nonlinear control theory for power system stability.

Tirasak Sapaklom received the B.Eng. degree (First Class Honours) and M.Eng. degrees in electrical engineering from the King Mongkut's University of Technology Thonburi, Bangkok, Thailand, in 2000 and 2003 respectively. He is Lecture with the Department of Electrical Engineering, King Mongkut's University of Technology Thonburi. His research interests include electric motor drives, power electronics circuit design and IoT Application in Electrical Engineering.

Mongkol Konghirun (Senior Member, IEEE) received the B.Eng. degree (First Class Honours) in electrical engineering from the King Mongkut's University of Technology Thonburi, Bangkok, Thailand, in 1995, and the M.Sc. and Ph.D. degrees in electrical engineering from The Ohio State University, Columbus, OH, USA, in 1999 and 2003, respectively. He is currently an Associate Professor with the Department of Electrical Engineering, King Mongkut's University of Technology Thonburi. His research interests include electric motor drives, motor designs, power electronics, transportation electrification, and renewable energy.